

Review

Application of Hot Isostatic Pressing in Nickel-Based Single Crystal Superalloys

Yunsong Zhao ¹, Siliang He ² and Longfei Li ^{2,3,*}

¹ Science and Technology on Advanced High Temperature Structural Materials Laboratory, AECC Beijing Institute of Aeronautical Materials, Beijing 100095, China; yunsong.zhao@biam.ac.cn

² State Key Laboratory for Advanced Metals and Materials, University of Science and Technology Beijing, Beijing 100083, China; he_siliang@xs.ustb.edu.cn

³ Beijing Key Laboratory of Special Melting and Reparation of High-End Metal Materials, University of Science and Technology Beijing, Beijing 100083, China

* Correspondence: lilf@skl.ustb.edu.cn

Abstract: Hot isostatic pressing (HIP) technology can effectively reduce microstructure defects such as micropores, which are formed during solidification and hominization heat treatment, and thus further improve the high temperature performance of nickel-based SX superalloys. This paper reviews the application of HIP treatment in nickel-based SX superalloys, focusing on the dislocation-creep closure and diffusion-creep closure mechanisms and the kinetics of annihilation of micropores by HIP. The effects of different scheme on pore closure and high temperature mechanical properties are compared. The advantages and disadvantages of different schemes are summarized. In addition, the application of HIP treatment in additive manufacturing (AM) of nickel-based SX superalloys is also discussed.

Keywords: nickel-based single crystal superalloy; HIP treatment; micropore; mechanical property; additive manufacturing



Citation: Zhao, Y.; He, S.; Li, L. Application of Hot Isostatic Pressing in Nickel-Based Single Crystal Superalloys. *Crystals* **2022**, *12*, 805. <https://doi.org/10.3390/cryst12060805>

Academic Editor: Pavel Lukáč

Received: 20 May 2022

Accepted: 1 June 2022

Published: 7 June 2022

Publisher's Note: MDPI stays neutral with regard to jurisdictional claims in published maps and institutional affiliations.



Copyright: © 2022 by the authors. Licensee MDPI, Basel, Switzerland. This article is an open access article distributed under the terms and conditions of the Creative Commons Attribution (CC BY) license (<https://creativecommons.org/licenses/by/4.0/>).

1. Introduction

Owing to the excellent combination of mechanical properties and environment resistance at high temperatures, nickel-based single crystal (SX) superalloys have been widely used for high-pressure turbine blades in aero-engines and industrial gas-turbines [1,2]. In comparison with other types of nickel-based superalloys, the most important characteristic of nickel-based SX superalloys is the elimination of grain boundaries which are quite weakened regions at high temperatures [3,4]. Commonly, nickel-based SX superalloys are fabricated by directional solidification casting, using Bridgman high-rate solidification (HRS) methods [5]. However, the application of this advanced technology cannot avoid detrimental microdefects, such as microporosity and residual eutectic, which would deteriorate the mechanical properties of nickel-based SX superalloy [6–11]. Moreover, in order to meet the increasing requirement of fuel efficiency and low emissions, more and more refractory elements, especially Re, are introduced in nickel-based SX superalloys for improving high temperature mechanical properties [12,13], such as creep resistance [14,15]. However, the higher contents of refractory elements would also increase the potential risk of detrimental microdefects [16].

In the mid-1950s, hot isostatic pressing (HIP) was developed by Battelle Institute, which applies high temperature and isostatic pressing to components. Owing to the unique advantage, HIP has been widely used in powder metallurgical applications to densify the materials [17–19] and even to near net shape forming [20–22], and for cast alloys to reduce the microporosity generated during the casting [23,24]. Nowadays, it has been well confirmed that HIP can significantly reduce the micro defects and improve the

homogenization of nickel-based SX superalloys, thus leading to the significant improvement of mechanical properties of nickel-based SX superalloys [7,23,25–32]. In general, there are mainly two schemes for the implementation of HIP within the standard heat treatment (SHT) for nickel-based SX superalloys, which consist of homogenization and aging treatment. Some works prefer the use of HIP after casting [30,31], while others prefer the incorporation after homogenization [23,33]. More recently, an integrated HIP heat-treatment was developed upon HIP equipment providing fast quenching rates [7,24,32,34].

Since these schemes produce quite different results about the effect of HIP on the mechanical properties of nickel-based SX superalloys, this article reviews the research progress in the application of HIP in nickel-based SX superalloys under different schemes, to promote the research in the application of HIP in the field of nickel-based SX superalloys.

2. Formation and Annihilation of Micropores in Nickel-Based SX Superalloys

2.1. Formation of Micropores

There are mainly two types of micropores after cast and standard heat treatment of nickel-based SX superalloy. The first one is the micropores formed during dendritic solidification of cast SX superalloys, called “S-pore”, which mainly come from two aspects. Firstly, the interdendritic liquid phase is isolated by the dendrite stem which has been completely solidified. The volume of the interdendritic liquid phase shrinks after solidification and cannot be supplemented by other liquid phases, thus forming irregular micropores in the interdendritic region. Secondly, due to the existence of partially dissolved gas in the liquid phase during solidification, spherical pores are formed after solidification [34–36]. Figure 1 shows a typical as-cast microstructure of a nickel-based SX superalloy, showing that micropores are mainly formed in the interdendritic region with a size of a few microns to a ten of microns.

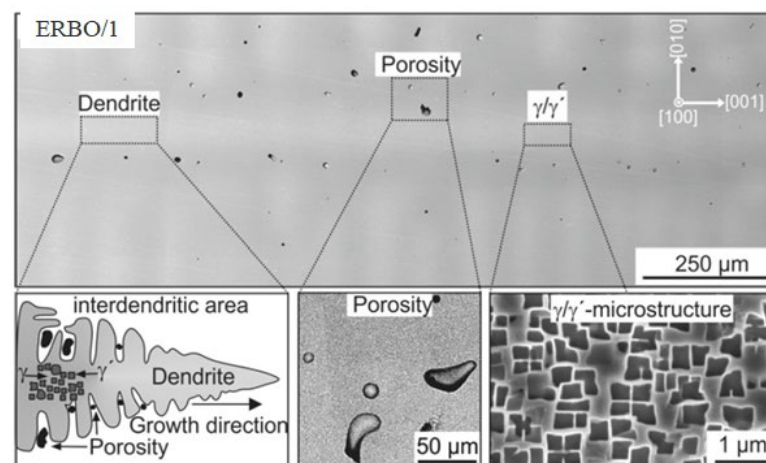


Figure 1. As-cast microstructure of nickel-based SX superalloy ERBO/1 [34].

The cooling rate has a significant effect on the formation of pores during solidification [35–37], as shown in Figure 2. When the cooling rate is 0.5 °C/s, the pore volume fraction is 0.22%, and is reduced to 0.14% with the cooling rate of 1 °C/s. In addition, at lower cooling rate, more small pores are produced at higher temperatures. The equivalent diameters of most of the pores are less than 10 μm and the sphericity index is greater than ~0.8, while larger pores tend to be more irregular and have a lower sphericity index. Therefore, increasing temperature gradient can significantly reduce the defect rate of single crystal blades. Compared with commonly used high rate solidification (HRS) process, the liquid metal cooling (LMC) process has a higher temperature gradient and the primary dendrite arm space (PDAS) after solidification is less than 400 μm, which is about 500 μm for HRS process, resulting in lower porosity than that of HRS process [37,38].

Nowadays, LMC process has been applied to the production of aviation blades and large gas turbine blades.

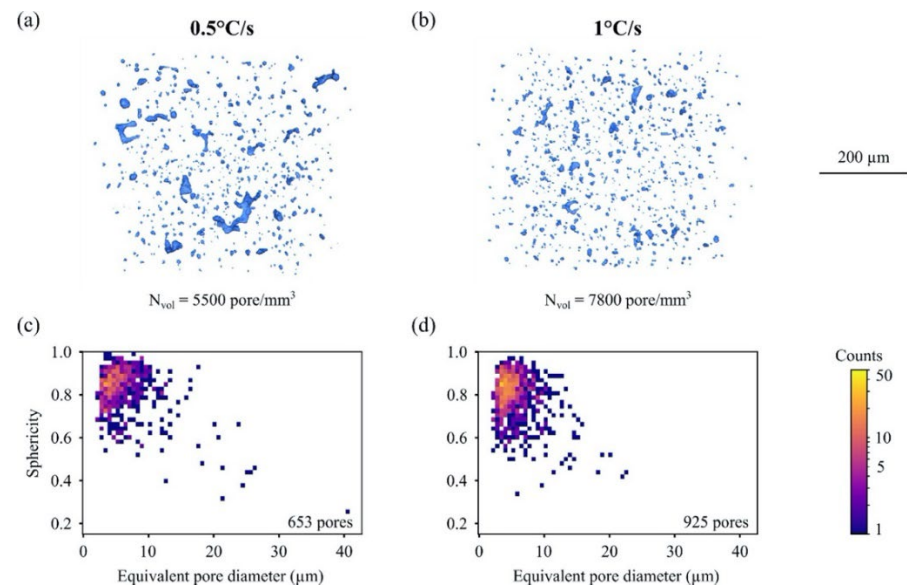


Figure 2. 3D view of the porosity after complete solidification for two cooling rates: (a) 0.5 °C/s and (b) 1 °C/s. The pore population in terms of size and sphericity for a cooling rate of (c) 0.5 °C/s and (d) 1 °C/s [36].

The second type of micropores is the micropores formed during homogenization heat treatment of as-cast SX superalloys, called “H-pore” [16,39,40]. The main reason is the dendrite-rich elements such as W, Re, Cr, and Co diffuse towards the interdendritic region, while interdendrite-rich elements such as Al and Ta diffuse towards the dendrite stems [41]. Kirkendal effect occurs due to different diffusion rates of these elements, resulting in approximately spherical solution pores in the interdendrite region, with a size of a few microns [42–44]. Especially, during homogenization heat treatment, the dissolution of Al-enriched residual eutectic located at the interdendrite region would lead to the diffusion of Al atoms into the surrounding matrix. Since the fast Al diffusion cannot be compensated by cross diffusion of other slower elements, H-pore is easy to form at the periphery of residual eutectic due to the reverse diffusion of matrix vacancy, as shown in Figure 3. In addition, the diffusion of matrix vacancy to the exiting S-pores would make them rounded, as shown in Figure 4 [24].

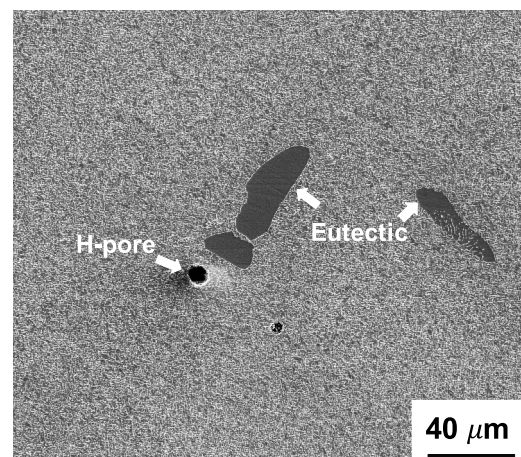


Figure 3. Homogenization pore grown near the eutectic in SX superalloy after standard heat treatment.

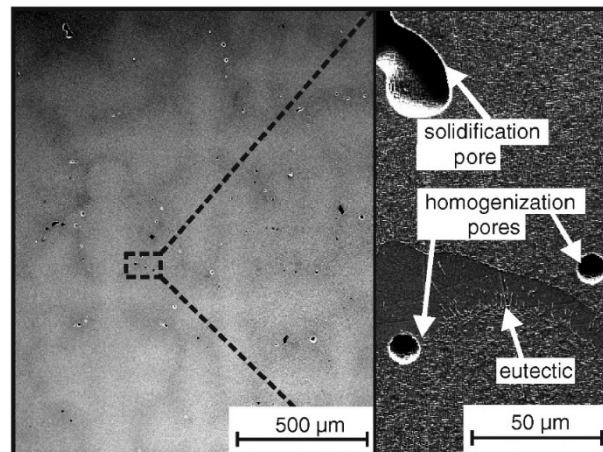


Figure 4. Morphology of micropores in SX superalloy ERBO/1 after heat treatment 1340 °C/16 h [24].

2.2. Annihilation of Micropores by HIP

S-pore and H-pore in nickel-based SX superalloys can be reduced by selecting the optimal parameters of directional solidification and homogenization heat treatment [16,36,45], but complete removal of the pores is only possible by applying a HIP treatment to the alloys. The annihilation of micropores by HIP is realized under the combining effect of high temperature and pressure [24,32,46,47]. Figure 5 shows the effect of temperature on the annihilation of micropores by HIP in SX superalloy ERBO/1 with different initial states [24]. It is clear that the efficiency of annihilation of micropores is low at temperatures under γ' -solvus temperature, due to the hardening effect of γ' phase, and is increased with increasing HIP temperature. At the temperature above γ' -solvus temperature, the initial porosity of the SX superalloy has been reduced by almost 100%.

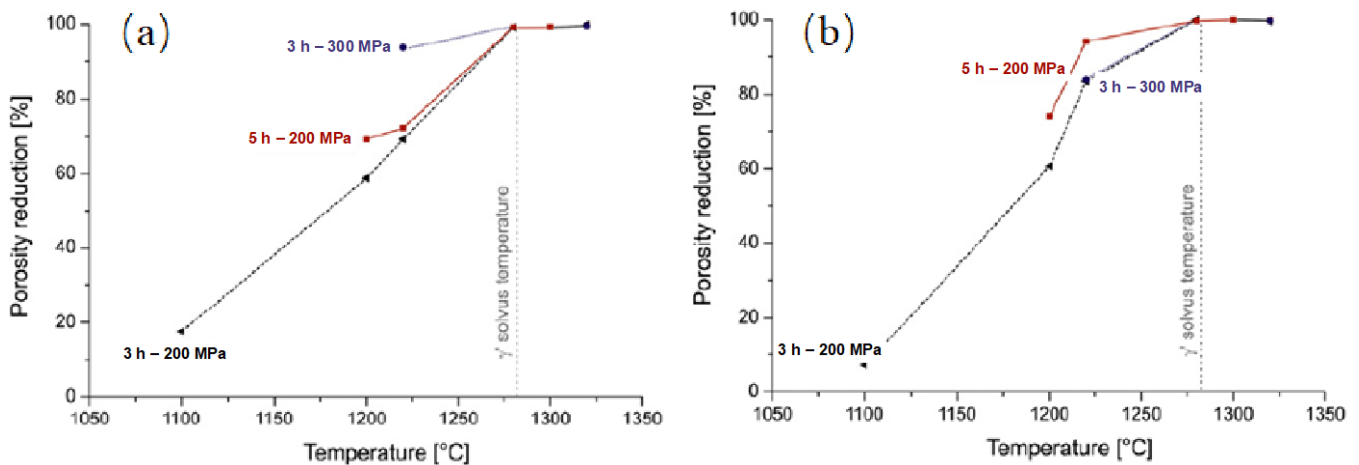


Figure 5. Effect of the temperature on the annihilation of micropores of (a) as-cast and (b) as-SHTed SX superalloy ERBO/1 [24].

Figure 6 shows the closure of pores in SX superalloy ERBO/1 after HIP at different conditions. At 1200 °C (below the γ' -solvus temperature, Figure 6a,b), a rafted structure can be observed around the pores that cover a radius of about 10 μm , which is the result of the local stress distribution during HIP. At 1300 °C, Figure 6a–d, no rafting is visible. The γ' -particles have dissolved during heat treatment, the dislocations are no longer pinned by γ' phase, and therefore the deformation can be expected to proceed more quickly. Meanwhile, the effect of pressure is not distinct as the temperature is above the γ' -solvus temperature; as shown in Figure 7a, 75 MPa is enough to reduce the porosity by 99%.

The deep understanding of the kinetics of annihilation of micropores during HIP is critical to the optimization of HIP parameters, such as temperature, pressure, and processing time. Figure 7b shows the porosity of nickel-based SX superalloy CMSX-4 in the as-cast, as-heat treated and as-HIPed states at different times, measured using light microscope (LM) and scanning electron microscope (SEM) as well as alloy density [48]. It clearly shows that the homogenization heat treatment can significantly increase the porosity of cast SX superalloy from ≈ 0.11 vol% (LM) to ≈ 0.20 vol% (LM) or ≈ 0.23 vol% (SEM). Meanwhile, HIP can dramatically eliminate porosity of heat-treated SX superalloy within a few hours.

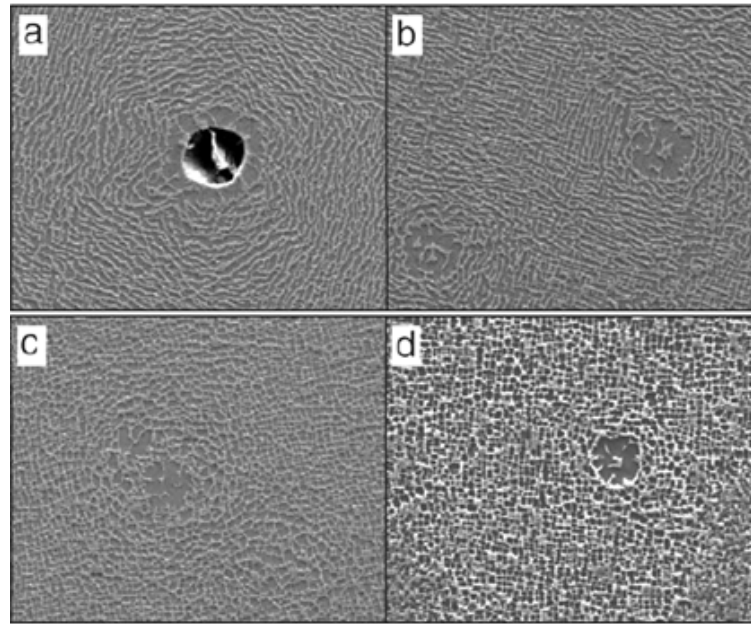


Figure 6. Pores closure in SX superalloy ERBO/1 after HIP at different conditions. (a,b) 200 MPa, 5 h, 1200 °C, and 10 K/min cooling rate; (c) 200 MPa, 5 h, 1300 °C, and 10 K/min cooling rate; (d) 100 MPa, 3 h, 1300 °C, and 20 K/min cooling rate [24].

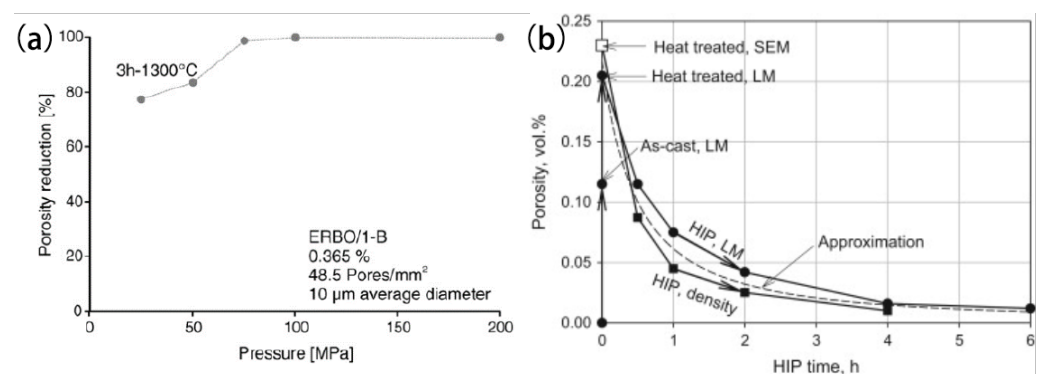


Figure 7. (a) Effect of the pressure on the annihilation of micropores of as- solutioning treated SX superalloy ERBO/1 [24]; (b) Porosity in as-cast and heat treated SX superalloy CMSX-4 and its annihilation during HIP at 1288 °C/103 MPa [48].

With TEM (transmission electron microscopy) results showing that the pores in SX superalloy CMSX-4 shrink via dislocation movement on octahedral glide planes during HIP, A. Epishin et al. [48] theoretically modeled pore closure under HIP conditions by the finite element method using crystal plasticity and large strain theories. As an example, in Figure 8, the pore has lost its sphericity and corners with large, localized plastic strains formed after treated by HIP for 10 min. The modeling gives a similar kinetics of pore

annihilation as observed experimentally, as shown in Figure 7, however, somewhat higher annihilation rate, as shown in Figure 9.

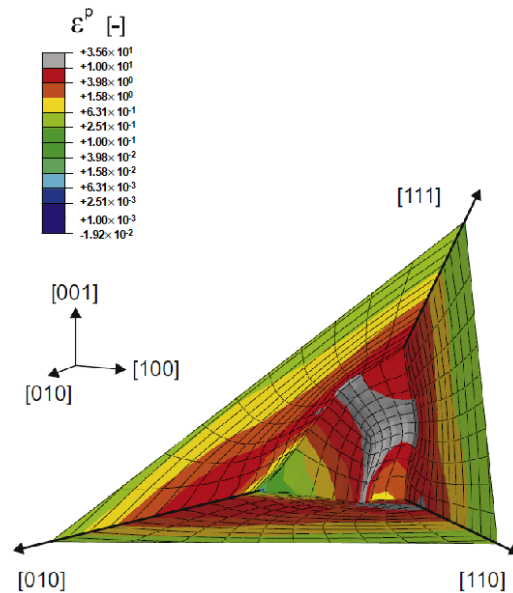


Figure 8. Distribution of equivalent plastic strains ε^P around the pore after HIP for 10 min [48].

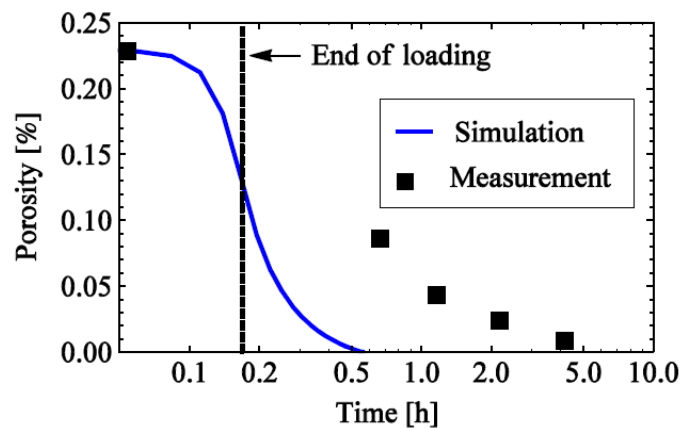


Figure 9. Kinetics of porosity decrease of SX superalloy CMSX-4 during HIP 1288 °C/103 MPa predicted by the modelling in comparison with the results of density measurements [48].

Afterwards, an improved diffusion model of pore annihilation during HIP of single crystals of nickel-based superalloys is proposed by A. Epishin et al. [45], based on the fact that a continuous γ' phase is formed around a pore and in the place of its annihilation as a result of inflow of rapidly diffusing aluminum atoms to the pore surface, as shown in Figure 6 and more clearly in Figure 10. Their model considers the dissolution of pores by emission of vacancies and their diffusion sink to low-angle boundaries, and takes into account pore size distribution, which is shown in Figure 11, and significantly influences the kinetics of pore annihilation. However, the result is still not very coincident with the experimental result, with a slower annihilation rate at the beginning. The deviation of these two models as mentioned above should come from the fact that the vacancy mechanism and dislocation mechanism should affect the pore closure simultaneously with different levels, as shown in Figure 12.

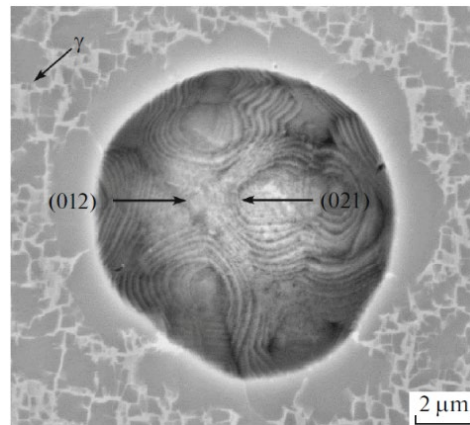


Figure 10. Pore faceted with {012} planes in SX superalloy CMSX-4 after 0.5 h of HIP at 1288 °C/103 MPa [45].

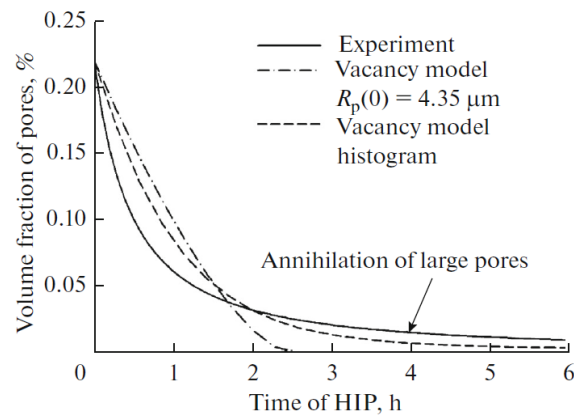


Figure 11. Kinetics of pore annihilation in heat-treated CMSX-4 alloy during HIP at 1288 °C/103 MPa [45].

To clarify the real mechanism of pore closure during HIP of nickel-based SX superalloy, further detailed investigation about local dislocation mechanisms and concentration micro gradients at the surface of partially shrank pores after HIP of limited duration should be carried out.

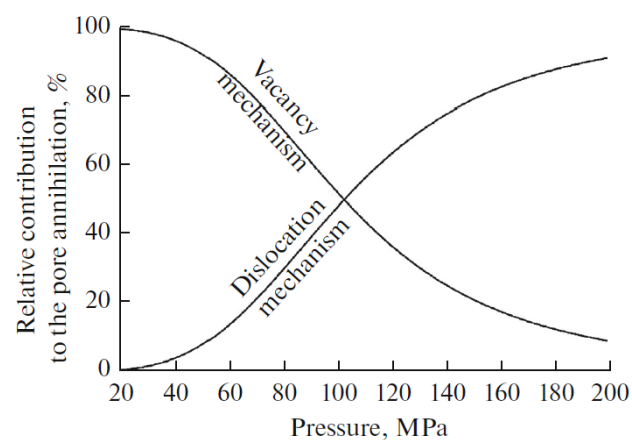


Figure 12. Change of relative contributions of vacancy and dislocation mechanisms to the pore annihilation during HIP with an increase in pressure [45].

2.3. Influence of HIP on Mechanical Properties

The implementation of HIP treatment in heat treatment process has a significant effect on high temperature mechanical properties of nickel-based SX superalloys. At present, due to considering that the HIP temperature is generally above the γ' -solution temperature [33], HIP treatment is generally performed directly on as-cast state nickel-based SX superalloys [28,30,31,49,50], which is equivalent to part of the solution treatment. By HIP, the internal pores and interdendritic eutectic are obviously reduced in nickel-based SX superalloys, which improves the fatigue performance but has no obvious effect on creep life at high temperatures [30,31]. As shown in Figure 13, after HIP treatment at 1300 °C/100 MPa for 4 h, the volume fraction of micropores decreased from 0.31% to 0.04% and the eutectic fraction also decreased significantly. Although the stress rupture life at 1100 °C/130 MPa was slightly changed, the low cycle fatigue life of the used SX superalloy at 760 °C was significantly increased by HIP, as shown showing in Figure 14 [30]. Furthermore, the high cycle fatigue life of the used nickel-based SX superalloy under 850 °C and 300 to 850 MPa was also improved significantly, and the fatigue strength was increased from 331 MPa to 433 MPa [31].

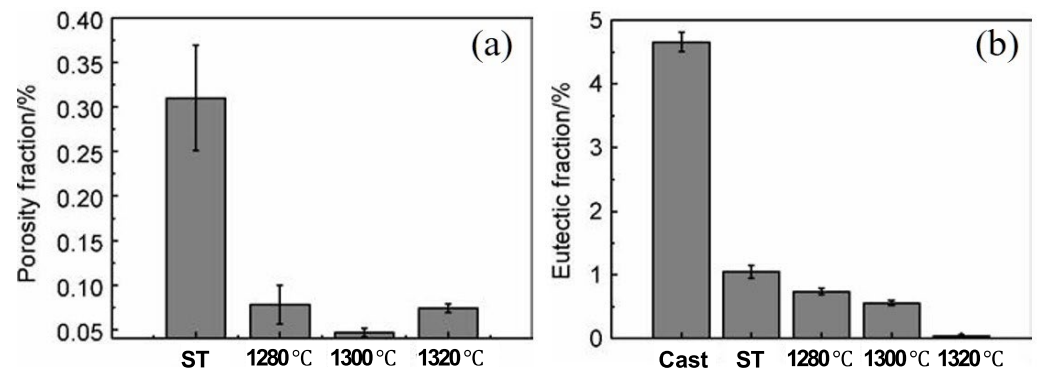


Figure 13. Micropore and eutectic content after HIP treatment with different temperature. (a) porosity fraction/%; (b) eutectic fraction/% [30].

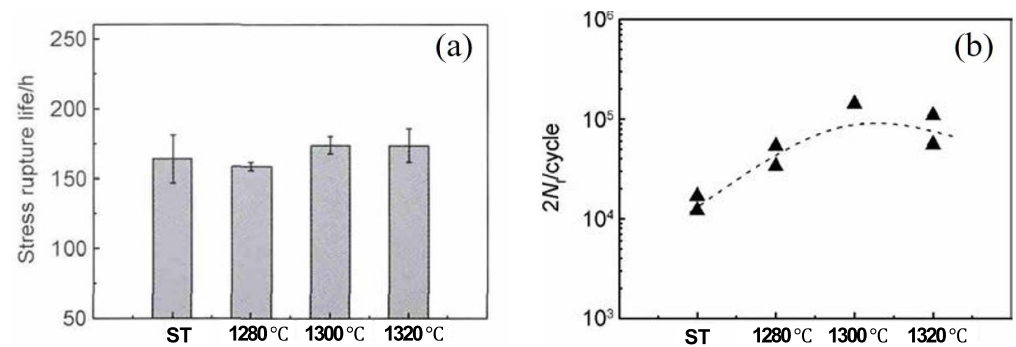


Figure 14. Micropore and eutectic content after HIP treatment with different temperature. (a) stress rupture life/h; (b) 2N_f cycles of 760 °C LCF, the 2N_f cycles of each state are tested once or twice, as shown in the black triangle [30].

R. C. Reed et al. [51] suggested that the formation of the TCP phase and the reappearance of micropores during creep at high temperature, as shown in Figure 15, would partially offset the closure of micropores by HIP treatment, and therefore the high temperature creep properties of nickel-based SX superalloys will be not improved obviously.

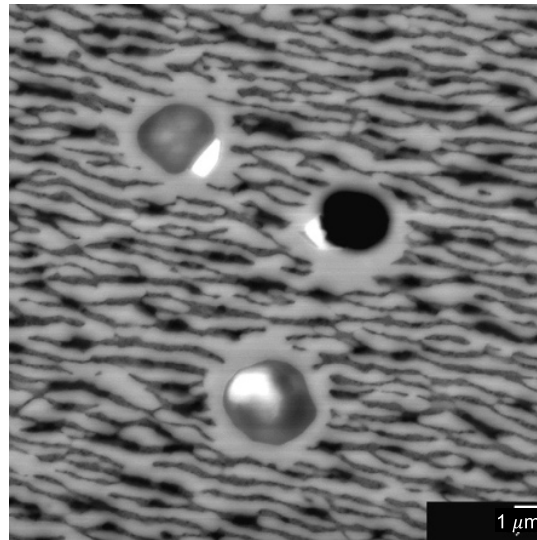


Figure 15. Backscattered electron image showing TCP phase particles and porosity in crept HIPed material [51].

However, direct HIP treatment on as-cast SX superalloy needs to avoid the occurrence of initial melting, so the increase of temperature of HIP is limited. As mentioned above, a higher temperature is necessary for HIP to the reduction of microporosity. In addition, the nucleation of pores in solid-solution and aging treatment after HIP would offset the reduction of porosity by HIP in nickel-based SX superalloys [42]. On the contrary, HIP treatment after solid-solution treatment has been found to effectively reduce the porosity in nickel-based SX superalloys, thus sufficiently improving the high temperature creep life of nickel-based SX superalloys [23,33]. Figure 16 shows that the high temperature creep life of nickel-based SX superalloy CMSX-4 can be significantly improved by over 80% in comparison with that of non-HIPed specimens, by HIP after solid-solution treatment [33].

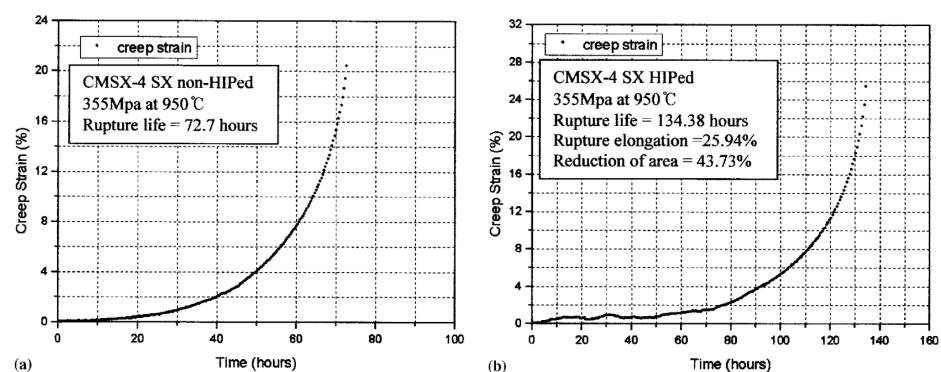


Figure 16. Stress-rupture curves of (a) non-HIP treated and (b) HIP treated [33].

Recently, the authors compared the two schemes of the implementation of HIP within the standard heat treatment (SHT) for a nickel-based SX superalloy with the as-cast or solid solution state. As shown in Figure 17, HIP treatment can effectively reduce the average size and fraction of micropores in as-cast and solid-solution states samples, especially for the solid-solution state sample. In addition, HIP can effectively reduce the interdendritic eutectic of as-cast and solution-state samples, but the solid-solution treatment can eliminate the interdendritic eutectic more significantly than HIP for higher temperature and longer time. As a result, the HIP treatment for the solid-solution state sample can significantly increase the high temperature stress rupture life of the nickel-based SX superalloy at 980 °C/250 MPa, as shown in Figure 17.

Figure 18 summarizes the mechanism of the two schemes on pore closure. In the as-cast state, eutectics distributes in the interdendritic region and enriches with Al, Ta elements, which will partially dissolve during HIP. Then, micropores will be generated during mutual diffusion of elements under Kirkendal–Frenkel effect, thus affecting the closure of micropores by HIP [23,52]. Meanwhile, in the solid-solution state, eutectics have dissolved, and HIP will lead to the closure of micropores which are formed either during the cast or during solid-solution treatment, thus showing high efficiency.

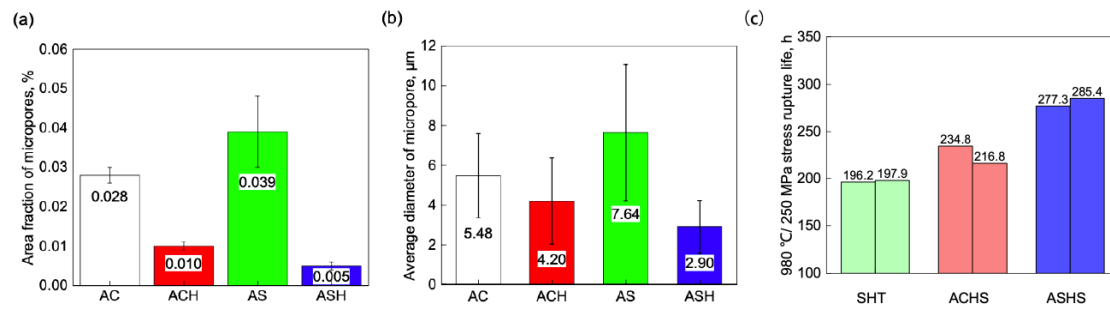


Figure 17. The diagrams of average area fractions and diameters of micropores. AC: as-cast state; ACH: as-cast + HIP state; AS: as-solid-solution state; ASH: as-solid-solution + HIP state. (a) Average area fraction of micropores; (b) Average diameter of micropores. (c) The high temperature stress rupture lives at 980 °C/250 MPa. SHT: the standard heat treatment without HIP; ACH: as-cast + HIP + SHT state; ASH: as-solid-solution + HIP + SHT state [23].

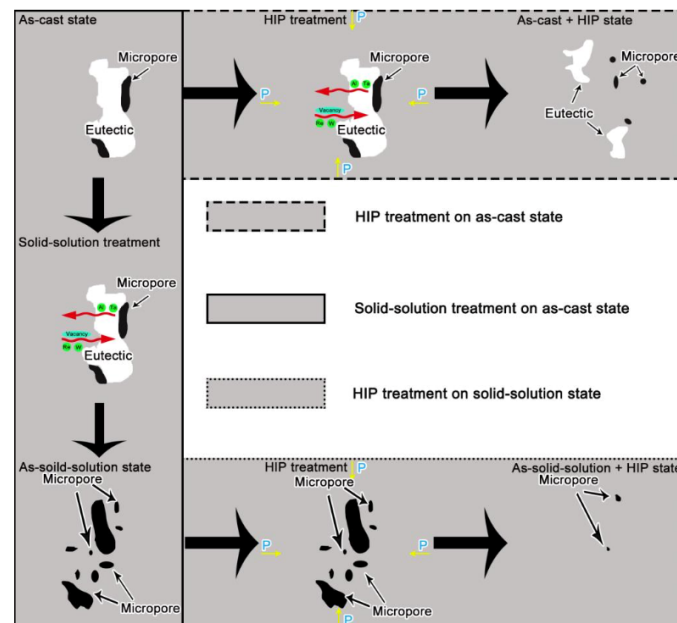


Figure 18. The changes of in interdendritic eutectic and micropores of used nickel-based SX superalloy under different states during HIP treatment [23].

However, both schemes for the implementation of HIP are somewhat complicated and costly, owing to the separation of HIP treatment and standard heat treatment. More recently, Luis Mujica Roncery et al. [32] developed an integrated HIP heat-treatment with the help of HIP equipment with a rapid cooling device, as shown in Figure 19. Such a scheme can overcome the shortage of these two schemes and set a fine and uniform γ/γ' -microstructure via fast quenching and subsequent aging, thus improving the mechanical properties of nickel-based SX superalloys significantly, as shown in Figure 20. It is worth mentioning that, although applying isostatic pressure throughout the standard heat treatment process

can significantly save the processing time and improve the creep properties, the scheme must have a HIP equipment with rapid cooling to obtain the appropriate microstructure.

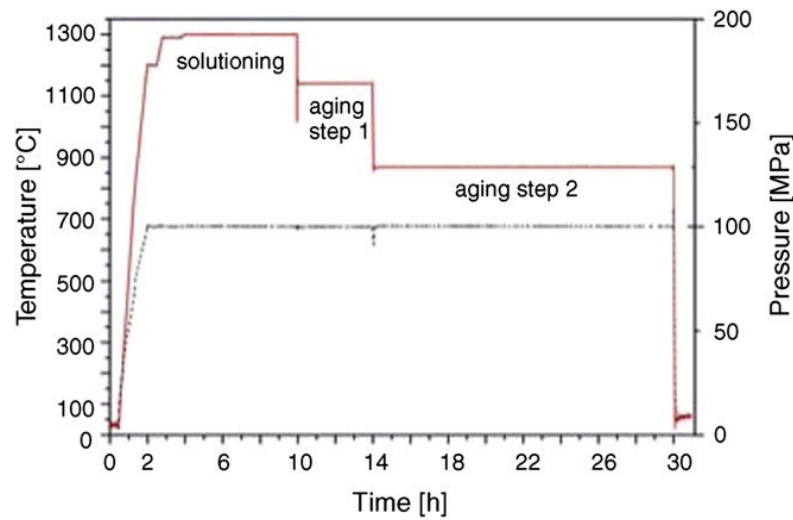


Figure 19. Profiles of the measured temperature (solid line) and pressure (dotted line) during the integrated HIP treatment that consisted of solutioning at 1300 °C and two-step aging at 1140 °C (4 h) and 870 °C (16 h), 100 MPa [32].

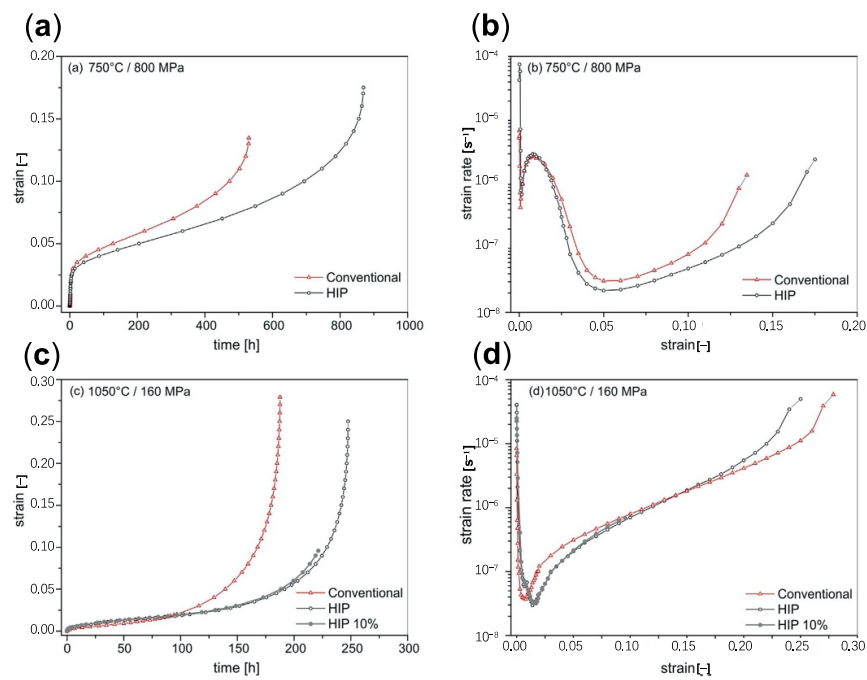


Figure 20. Creep data from five creep experiments performed in the present study. (a,b) 750 °C, 800 MPa. (c,d) 1050 °C, 160 MPa. (a,c) Strain versus time. (b,d) Creep rate plotted as a function of strain [32].

2.4. Application of HIP in Additive Manufacturing of Nickel-Based Superalloys

Besides directional solidification casting, additive manufacturing (AM) is another potential process for fabricating nickel-based SX superalloys. AM technology is gaining increasing attention from industry, owing to its superiority in direct fabrication of components with extremely complex internal structures, e.g., turbine blades with inner cooling channels. Currently, many printing trials with nickel-based superalloys are being conducted by researchers, and samples and components have been successfully fabricated [53–65].

The nickel-based superalloy has a severe crack tendency in the laser powder bed fusion (L-PBF) process, which hinders its wide application in aerospace field. Figure 21 shows that HIP can reduce the volume fraction of pores and microcracks from 0.96% to 0.08%. After subsequent heat treatment (HIP+SSHT), although cracks did not reappear after subsequent heat treatment, the volume fraction of pores slightly increased. In addition, sub-grain with high-density dislocations can be reduced by HIP treatment with high temperature and after subsequent heat treatment it was eliminated. Finally, the tensile properties in room temperature and 900 °C were both improved compared to the as-built state.

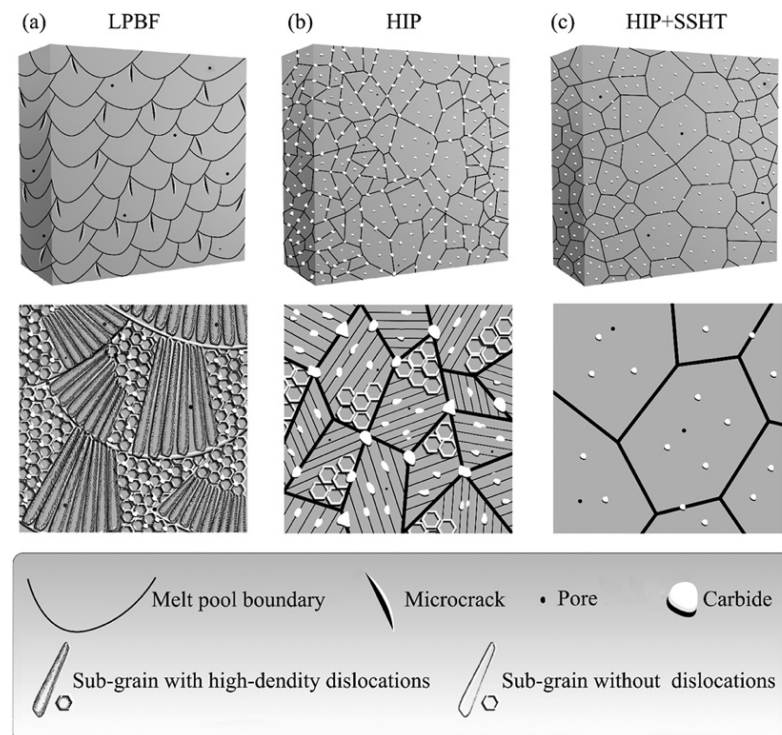


Figure 21. Microstructure development schematic of the LPBF GH3536 sample subjected to the HIP and SSHT. (a) The as-built state after L-PBF process. (b) After HIP treatment. (c) After SSHT treatment [62].

Some works are pursuing a methodology of producing components of SX nickel-based superalloys [66–68]. Owing to the nonequilibrium fusion-solidification characteristic of AM process, the primary dendrite arm spacing (PDAS) of as-built SX superalloy by electron beam powder bed fusion (EB-PBF) is quite smaller than that of traditional as-cast one [69]. Thus, as shown in Figure 22, the chemical compositions of the crack-free CMSX-4 SX samples built by EB-PBF were homogeneous with two orders of magnitude smaller than that of traditional castings. HIP treatment can further reduce the internal pores of the as-built sample and improve the homogenization of alloying elements. For nickel-based superalloy CMSX-4 prepared by SEBM, only after 4 min of HIP treatment at 1300 °C, the alloy density increased to 99.9%, and the homogenization degree of dendrite composition of the as-built state was obviously improved [67], as shown in Figure 23. Such special characteristic of additive manufactured SX superalloy improves the fatigue properties significantly [70], as shown in Figure 24. L. M. Bortoluci Ormastroni et al. [66] also reported that the very high cycle fatigue (VHCF) lifetime of SX superalloy CMSX-4 fabricated by EB-PBF with complete elimination of defects is equivalent to or higher than that of Bridgman solidified Ni-based SX superalloys. What is more, after HIP treatment, all EB-PBF samples without defects failed through oxidation assisted surface crack initiation.

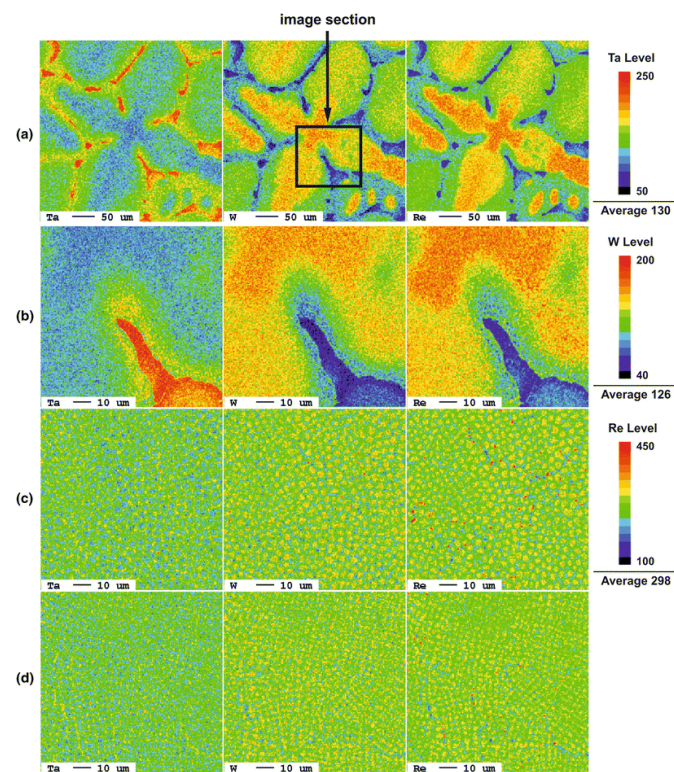


Figure 22. Qualitative microprobe mappings (horizontal cross section) of Ta, W, and Re: (a) as-cast sample analyzed with a spot size of 2 μm ; (b) Magnification of (a) (spot size 0.5 μm); (c) EB-PBF sample ($P = 510$ W, $v = 6000$ mm/s, line offset = 0.03 mm) (spot size 0.5 μm); (d) EB-PBF sample ($P = 180$ W, $v = 300$ mm/s, line offset = 0.1 mm) (spot size 0.5 μm) [69].

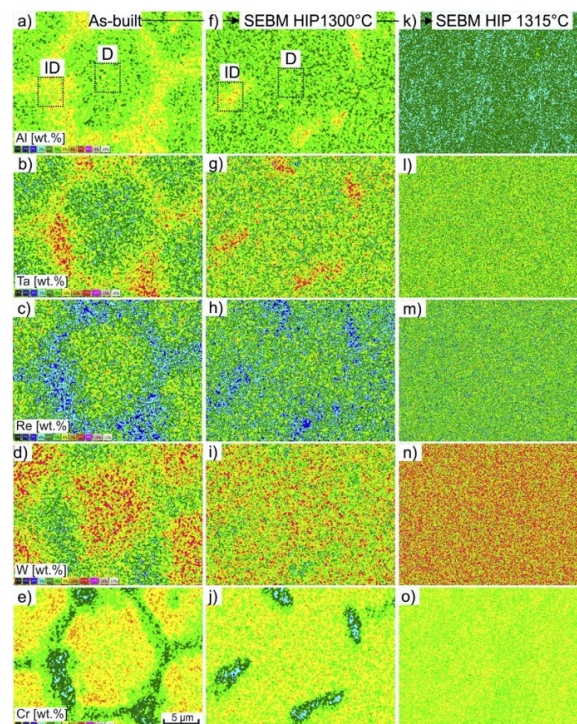


Figure 23. EDS element mappings of the SEBM material in the as-built state (a–e) and after two (f–j,k–o) different subsequent HIP treatments [67].

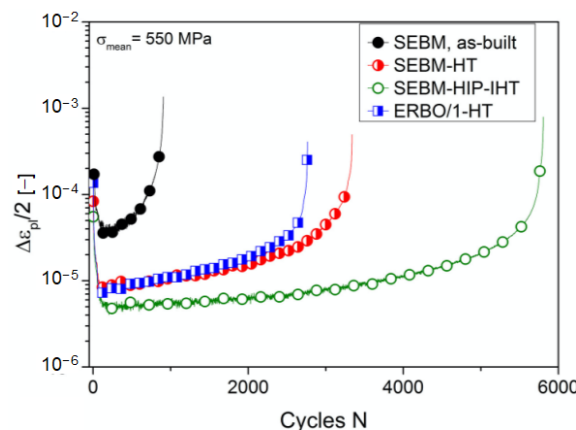


Figure 24. Results of low cycle fatigue (LCF) experiments on different heat treated specimens of nickel-based SX superalloy [70].

As an emerging technology, AM has promising application prospects for the fabrication of SX superalloys, and HIP has become a common process for as-built superalloys prepared by AM prior to heat treatment. It should be noted that, the recrystallization may occur during high-temperature HIP treatment [71], which has a certain influence on the high-temperature strength of SX superalloys, due to the large residual stress in the as-built samples. The application of HIP in the additive manufacturing of nickel-based SX superalloys should be carefully implemented.

3. Summary

With the rapid development of modern advanced aero-engines and industrial gas-turbines, the demand for the service security and reliability of nickel-based SX superalloys is constantly increasing. Therefore, HIP treatment is more widely used in the fabrication of nickel-based SX components, and there are mainly three schemes for the implementation of HIP within the standard heat treatment (SHT) of nickel-based SX superalloys. The normal scheme is the use of HIP after casting, followed by SHT. It is relatively easy with a low efficiency of pore closure. The second one is the incorporation of HIP after homogenization, followed by an additional short homogenization and aging treatment. It is relatively complicated but with a high efficiency of pore closure. The third one is the integrated HIP heat-treatment, i.e., the incorporation of HIP during SHT. It is quite efficient but upon special HIP equipment providing fast quenching rates.

In order to give full play to the comprehensive properties of the material, the influence of HIP parameters on microstructures and mechanical properties of nickel-based SX superalloys, including temperature, pressure, holding time, heating rate, and cooling rate, has been widely investigated. However, the model of annihilation of micropores by HIP is not developed well enough, and thus limits the optimization of the implementation of HIP within the standard heat treatment (SHT) for nickel-based SX superalloys. Further investigation should be conducted with the help of in-situ experimental methods.

Furthermore, additive manufacturing (AM) provides new possibilities for the preparation and processing of advanced aero-engine materials and HIP treatment has inherent advantages in improving the quality of SX components fabricated by AM. The implementation of HIP in AM field is the direction to be urgently solved in the future.

Author Contributions: Conceptualization, review and editing, Y.Z.; Review and investigation, L.L. and S.H. All authors have read and agreed to the published version of the manuscript.

Funding: This review was supported by the National Natural Science Foundation of China (Grant No.: 52001297, 91860201), National Science and Technology Major Project (Grant No.:2017-VI-0002-0072), and 111 Project (Grant No.: B170003).

Acknowledgments: The authors would like to acknowledge the supports provided by Jian Zhang from AECC Beijing Institute of Aeronautical Materials for the help of revising.

Conflicts of Interest: The authors declare no conflict of interest.

References

1. Rame, J.; Utada, S.; Bortoluci Ormastroni, L.M.; Mataveli-Suave, L.; Menou, E.; Després, L.; Kontis, P.; Cormier, J. Platinum-containing new generation nickel-based superalloy for single crystalline applications. In *Superalloys 2020*; Springer: Berlin/Heidelberg, Germany, 2020; pp. 71–81.
2. Kool, G. *Current and Future Materials in Advanced Gas Turbine Engines*; Citeseer: University Park, PA, USA, 1994; Volume 78873.
3. Zhao, Y.; Zhang, J.; Luo, Y.; Zhang, B.; Sha, G.; Li, L.; Tang, D.; Feng, Q. Improvement of grain boundary tolerance by minor additions of Hf and B in a second generation single crystal superalloy. *Acta Mater.* **2019**, *176*, 109–122. [[CrossRef](#)]
4. Ma, X.; Jiang, J.; Zhang, W.; Shi, H.-J.; Gu, J. Effect of local recrystallized grains on the low cycle fatigue behavior of a nickel-based single crystal superalloy. *Crystals* **2019**, *9*, 312. [[CrossRef](#)]
5. Han, D.; Jiang, W.; Xiao, J.; Li, K.; Lu, Y.; Zheng, W.; Zhang, S.; Lou, L. Investigation on freckle formation and evolution of single-crystal nickel-based superalloy specimens with different thicknesses and abrupt cross-section changes. *J. Alloys Compd.* **2019**, *805*, 218–228. [[CrossRef](#)]
6. Huang, Y.; Wang, D.; Shen, J.; Lu, Y.; Lou, L.; Zhang, J. Initiation of fatigue cracks in a single-crystal nickel-based superalloy at intermediate temperature. In *Superalloys 2020*; Springer: Berlin/Heidelberg, Germany, 2020; pp. 208–217.
7. Rutttert, B.; Meid, C.; Roncery, L.M.; Lopez-Galilea, I.; Bartsch, M.; Theisen, W. Effect of porosity and eutectics on the high-temperature low-cycle fatigue performance of a nickel-base single-crystal superalloy. *Scr. Mater.* **2018**, *155*, 139–143. [[CrossRef](#)]
8. Buck, H.; Wollgramm, P.; Parsa, A.; Eggeler, G. A quantitative metallographic assessment of the evolution of porosity during processing and creep in single crystal Ni-base super alloys: Eine quantitative metallographische Abschätzung der Porenentwicklung bei der Herstellung und beim Kriechen von einkristallinen Nickelbasis-Superlegierungen. *Materialwissenschaft und Werkstofftechnik* **2015**, *46*, 577–590.
9. Seo, S.M.; Lee, J.H.; Yoo, Y.S.; Jo, C.Y.; Miyahara, H.; Ogi, K. A Comparative Study of the γ/γ' Eutectic Evolution during the Solidification of Ni-Base Superalloys. *Metall. Mater. Trans. A* **2011**, *42*, 3150–3159. [[CrossRef](#)]
10. Ashbrook, R.L. Directionally solidified ceramic eutectics. *J. Am. Ceram. Soc.* **2010**, *60*, 428–435. [[CrossRef](#)]
11. Whitesell, H.S.; Overfelt, R.A. Influence of solidification variables on the microstructure, macrosegregation, and porosity of directionally solidified Mar-M247. *Mater. Sci. Eng. A* **2001**, *318*, 264–276. [[CrossRef](#)]
12. Heckl, A.; Rettig, R.; Singer, R. Solidification characteristics and segregation behavior of nickel-base superalloys in dependence on different rhenium and ruthenium contents. *Metall. Mater. Trans. A* **2010**, *41*, 202. [[CrossRef](#)]
13. Lamm, M.; Singer, R. The effect of casting conditions on the high-cycle fatigue properties of the single-crystal nickel-base superalloy PWA 1483. *Metall. Mater. Trans. A* **2007**, *38*, 1177–1183. [[CrossRef](#)]
14. Lu, F.; Antonov, S.; Lu, S.; Zhang, J.; Li, L.; Wang, D.; Zhang, J.; Feng, Q. Unveiling the Re effect on long-term coarsening behaviors of γ' precipitates in Ni-based single crystal superalloys. *Acta Mater.* **2022**, *23*, 117979. [[CrossRef](#)]
15. Lu, F.; Li, L.; Antonov, S.; Zheng, Y.; Fraser, H.L.; Wang, D.; Zhang, J.; Feng, Q. Effect of Re on Long-Term Creep Behavior of Nickel-Based Single-Crystal Superalloys for Industrial Gas Turbine Applications. In *Superalloys 2020*; Springer: Berlin/Heidelberg, Germany, 2020; pp. 218–227.
16. Zhang, Y.; Huang, T.; Zhou, Z.; Li, M.; Tan, L.; Gan, B.; Jie, Z.; Qin, L.; Zhang, J.; Liu, L. Variation of Homogenization Pores during Homogenization for Nickel-Based Single-Crystal Superalloys. *Adv. Eng. Mater.* **2021**, *23*, 2001547. [[CrossRef](#)]
17. Teng, Q.; Xie, Y.; Sun, S.; Xue, P.; Long, A.; Wu, T.; Cai, C.; Guo, J.; Wei, Q. Understanding on processing temperature-metallographic microstructure-tensile property relationships of third-generation nickel-based superalloy WZ-A3 prepared by hot isostatic pressing. *J. Alloys Compd.* **2022**, *909*, 164668. [[CrossRef](#)]
18. Sun, D.; Zhao, K.; Li, G.; Kang, J.; Gao, K.; Zhang, Z.; Gao, Y.; Fan, L.; An, L. Hot oscillating pressed FGH4096 nickel-based alloy with enhanced ductility and strength. *J. Alloys Compd.* **2022**, *894*, 162366. [[CrossRef](#)]
19. Weddeling, A.; Theisen, W. Energy and time saving processing: A combination of hot isostatic pressing and heat treatment. *Metal. Powder Rep.* **2017**, *72*, 345–348. [[CrossRef](#)]
20. Sergi, A.; Khan, R.H.; Attallah, M.M. The role of powder atomisation route on the microstructure and mechanical properties of hot isostatically pressed Inconel 625. *Mater. Sci. Eng. A* **2021**, *808*, 140950. [[CrossRef](#)]
21. Qin, S.; Yan, L.; Zhang, X. Eliminating topologically closed-packed phases in deteriorated nickel-based superalloy by pulsed electric current. *J. Alloys Compd.* **2021**, *862*, 158508. [[CrossRef](#)]
22. Bai, J.; Xing, P.; Zhang, H.; Li, X.; Liu, J.; Jia, J.; Sun, Q.; Liu, C.; Zhang, Y. Effect of tantalum on the microstructure stability of PM Ni-base superalloys. *Mater. Charact.* **2021**, *179*, 111326. [[CrossRef](#)]
23. He, S.; Zhao, Y.; Lu, F.; Zhang, J.; Li, L.; Feng, Q. Effects of Hot Isostatic Pressure on Microdefects and Stress Rupture Life of Second-Generation Nickel-Based Single Crystal Superalloy in As-Cast and As-Solid-Solution States. *Acta Metall. Sin.* **2020**, *56*, 1195–1205.
24. Roncery, L.M.; Lopez-Galilea, I.; Rutttert, B.; Huth, S.; Theisen, W. Influence of temperature, pressure, and cooling rate during hot isostatic pressing on the microstructure of an SX Ni-base superalloy. *Mater. Des.* **2016**, *97*, 544–552. [[CrossRef](#)]

25. Fritzscheier, L. The influence of high thermal gradient casting, hot isostatic pressing and alternate heat treatment on the structure and properties of a single crystal nickel base superalloy. *Superalloys* **1988**, *1998*, 265–274.
26. Zou, J.-W.; Wang, W.-X. Development and application of P/M superalloy. *J. Aeronaut. Mater.* **2006**, *26*, 244–250.
27. Zhou, Y.; Zhang, Z.; Zhong, Q.; Zhao, Z. Model for healing of creep cavities in nickel-based superalloys under hot isostatic pressing. *Comput. Mater. Sci.* **2012**, *65*, 320–323. [[CrossRef](#)]
28. Liu, L.J.; Xue, M.; Chen, J.Y.; Cao, L.M. Effect of Hot Isostatic Pressing on the Microstructure of Single Crystal Ni-Based Superalloy DD10. *Mater. Sci. Forum* **2013**, *747*, 772–776. [[CrossRef](#)]
29. Yu, Z.; Rao, S.; Zheng, Z.; Zhao, Z. Interaction of hot isostatic pressing temperature and hydrostatic pressure on the healing of creep cavities in a nickel-based superalloy. *Mater. Des.* **2013**, *49*, 25–27.
30. Guo, H.M.; Zhao, Y.S.; Zheng, S.; Xu, J.W.; Zhang, J.; Luo, Y.S.; Dong, J.X. Effect of Hot-Isostatic Pressing on Microstructure and Mechanical Properties of Second Generation Single Crystal Superalloy DD6. *J. Mater. Eng. Perform.* **2016**, *44*, 60–67.
31. Luo, Y.S.; Guo, H.M.; Zhao, Y.S.; Zhang, J. Effect of Hot Isostatic Pressing on High-Temperature High Cycle Fatigue Properties of a Second Generation Single Crystal Superalloy DD6. *Mater. Mech. Eng.* **2016**, *40*, 51–118.
32. Roncery, L.M.; Lopez-Galilea, I.; Rutttert, B.; Buerger, D.; Wollgramm, P.; Eggeler, G.; Theisen, W. On the effect of hot isostatic pressing on the creep life of a single crystal superalloys. *Adv. Eng. Mater.* **2016**, *18*, 1381–1387. [[CrossRef](#)]
33. Chang, J.C.; Choi, C.; Kim, J.C.; Yun, Y.H. Development of microstructure and mechanical properties of a Ni-base single-crystal superalloy by hot-isostatic pressing. *J. Mater. Eng. Perform.* **2003**, *12*, 420–425. [[CrossRef](#)]
34. Rutttert, B.; Lopez-Galilea, I.; Theisen, W. An integrated HIP heat-treatment of a single crystal Ni-base superalloy. In *Superalloys 2020*; Springer: Berlin/Heidelberg, Germany, 2020; pp. 391–399.
35. Qianying, S.; Xianghui, L.I.; Yunrong, Z.; Guang, X.; Jian, Z.; Qiang, F. Formation of Solidification and Homogenisation Micropores in Two Single Crystal Superalloys Produced by HRS and LMC Processes. *Acta Metall. Sin.* **2012**, *48*, 1237–1247.
36. Plancher, E.; Gravier, P.; Chauvet, E.; Blandin, J.J.; Lhuissier, P. Tracking pores during solidification of a Ni-based superalloy using 4D synchrotron microtomography. *Acta Mater.* **2019**, *181*, 1–9. [[CrossRef](#)]
37. Zhang, J.; Wang, L.; Wang, D.; Xie, G.; Lu, Y.; Shen, J.; Lou, L. Recent progress in research and development of nickel-based single crystal superalloys. *Acta Metall. Sin.* **2019**, *55*, 1077–1094.
38. Konter, M. A Novel Casting Process for Single Crystal Gas Turbine Components. In *Superalloys 2000*; Springer: Berlin/Heidelberg, Germany, 2000.
39. Hegde, S.; Kearsey, R.; Beddoes, J. Designing homogenization–solution heat treatments for single crystal superalloys. *Mater. Sci. Eng. A* **2010**, *527*, 5528–5538. [[CrossRef](#)]
40. Li, X.; Wang, L.; Dong, J.; Lou, L.; Zhang, J. Evolution of micro-pores in a single-crystal nickel-based superalloy during solution heat treatment. *Metall. Mater. Trans. A* **2017**, *48*, 2682–2686. [[CrossRef](#)]
41. Karunaratne, M.; Cox, D.; Carter, P.; Reed, R. Modelling of the microsegregation in CMSX-4 superalloy and its homogenisation during heat treatment. In *Superalloys 2000*; Springer: Berlin/Heidelberg, Germany, 2000; pp. 263–272.
42. Anton, D.L.; Giamei, A.F. Porosity distribution and growth during homogenization in single crystals of a nickel-base superalloy. *Mater. Sci. Eng.* **1985**, *76*, 173–180. [[CrossRef](#)]
43. Bokstein, B.S.; Epishin, A.I.; Link, T.; Esin, V.A.; Rodin, A.O.; Svetlov, I.L. Model for the porosity growth in single-crystal nickel-base superalloys during homogenization. *Scr. Mater.* **2007**, *57*, 801–804. [[CrossRef](#)]
44. Epishin, A.; Link, T.; Svetlov, I.L.; Nolze, G.; Neumann, R.S.; Lucas, H. Mechanism of porosity growth during homogenisation in single crystal nickel-based superalloys. *Int. J. Mater. Res.* **2013**, *104*, 776–782. [[CrossRef](#)]
45. Epishin, A.I.; Bokstein, B.S.; Svetlov, I.L.; Fedelich, B.; Feldmann, T.; Le Bouar, Y.; Ruffini, A.; Finel, A.; Viguier, B.; Poquillon, D. A vacancy model of pore annihilation during hot isostatic pressing of single crystals of nickel-base superalloys. *Inorg. Mater. Appl. Res.* **2018**, *9*, 57–65. [[CrossRef](#)]
46. Wei, C.-N.; Bor, H.-Y.; Chang, L. Effect of hot isostatic pressing on microstructure and mechanical properties of CM-681LC nickel-base superalloy using microcast. *Mater. Trans.* **2008**, *49*, 193–201. [[CrossRef](#)]
47. Zhao, X.; Lin, X.; Chen, J.; Xue, L.; Huang, W. The effect of hot isostatic pressing on crack healing, microstructure, mechanical properties of Rene88DT superalloy prepared by laser solid forming. *Mater. Sci. Eng. A* **2009**, *504*, 129–134. [[CrossRef](#)]
48. Epishin, A.; Fedelich, B.; Link, T.; Feldmann, T.; Svetlov, I.L. Pore annihilation in a single-crystal nickel-base superalloy during hot isostatic pressing: Experiment and modelling. *Mater. Sci. Eng. A* **2013**, *586*, 342–349. [[CrossRef](#)]
49. Bor, H.; Hsu, C.; Wei, C. Influence of hot isostatic pressing on the fracture transitions in the fine grain MAR-M247 superalloys. *Mater. Chem. Phys.* **2004**, *84*, 284–290. [[CrossRef](#)]
50. Kim, M.; Chang, S.; Won, J. Effect of HIP process on the micro-structural evolution of a nickel-based superalloy. *Mater. Sci. Eng. A* **2006**, *441*, 126–134. [[CrossRef](#)]
51. Reed, R.C.; Cox, D.C.; Rae, C.M.F. Damage accumulation during creep deformation of a single crystal superalloy at 1150 °C. *Mater. Sci. Eng. A* **2007**, *448*, 88–96. [[CrossRef](#)]
52. Paraschiv, A.; Matache, G.; Puscasu, C. The effect of heat treatment on the homogenization of CMSX-4 Single-Crystal Ni-Based Superalloy. *Transp. Res. Procedia* **2018**, *29*, 303–311. [[CrossRef](#)]
53. Chittewar, S.L.; Patil, N.G. Surface integrity of conventional and additively manufactured nickel superalloys: A review. *Mater. Today Proc.* **2021**, *44*, 701–708. [[CrossRef](#)]

54. Neikter, M.; Raja, D.; Balachandramurthi, A.R.; Harlin, P. Tailored ductility and strength for enhanced impact toughness of laser powder fusion built Alloy 718. *J. Alloys Compd.* **2021**, *884*, 161374. [[CrossRef](#)]
55. Markanday, J.; Carpenter, M.; Jones, N.; Thompson, R.; Rhodes, S.; Heason, C.; Stone, H. Occurrence of a brass texture and elastic anisotropy in laser blown powder processed superalloy IN718. *Mater. Sci. Eng. A* **2021**, *825*, 141781. [[CrossRef](#)]
56. Peng, H.; Shi, Y.; Gong, S.; Guo, H.; Chen, B. Microstructure, mechanical properties and cracking behaviour in a γ' -precipitation strengthened nickel-base superalloy fabricated by electron beam melting. *Mater. Des.* **2018**, *159*, 155–169. [[CrossRef](#)]
57. Montero-Sistiaga, M.L.; Pourbabak, S.; Van Humbeeck, J.; Schryvers, D.; Vanmeensel, K. Microstructure and mechanical properties of Hastelloy X produced by HP-SLM (high power selective laser melting). *Mater. Des.* **2019**, *165*, 107598. [[CrossRef](#)]
58. Khomutov, M.; Potapkin, P.; Cheverikin, V.; Petrovskiy, P.; Travyanov, A.; Logachev, I.; Sova, A.; Smurov, I. Effect of hot isostatic pressing on structure and properties of intermetallic NiAl–Cr–Mo alloy produced by selective laser melting. *Intermetallics* **2020**, *120*, 106766. [[CrossRef](#)]
59. Lee, J.-U.; Kim, Y.-K.; Seo, S.-M.; Lee, K.-A. Effects of hot isostatic pressing treatment on the microstructure and tensile properties of Ni-based superalloy CM247LC manufactured by selective laser melting. *Mater. Sci. Eng. A* **2022**, *841*, 143083. [[CrossRef](#)]
60. Deshpande, A.; Deb Nath, S.; Atre, S.; Hsu, K. Effect of post processing heat treatment routes on microstructure and mechanical property evolution of Haynes 282 Ni-based superalloy fabricated with selective laser melting (SLM). *Metals* **2020**, *10*, 629. [[CrossRef](#)]
61. Seidel, A.; Finaske, T.; Straubel, A.; Wendrock, H.; Maiwald, T.; Riede, M.; Lopez, E.; Brueckner, F.; Leyens, C. Additive manufacturing of powdery Ni-based superalloys Mar-M-247 and CM 247 LC in hybrid laser metal deposition. *Metall. Mater. Trans. A* **2018**, *49*, 3812–3830. [[CrossRef](#)]
62. Sun, S.; Teng, Q.; Xie, Y.; Liu, T.; Ma, R.; Bai, J.; Cai, C.; Wei, Q. Two-step heat treatment for laser powder bed fusion of a nickel-based superalloy with simultaneously enhanced tensile strength and ductility. *Addit. Manuf.* **2021**, *46*, 102168. [[CrossRef](#)]
63. Goel, S.; Mehtani, H.; Yao, S.-W.; Samajdar, I.; Klement, U.; Joshi, S. As-built and post-treated microstructures of an electron beam melting (EBM) produced nickel-based superalloy. *Metall. Mater. Trans. A* **2020**, *51*, 6546–6559. [[CrossRef](#)]
64. Pei, C.; Yuan, H.; Li, B.; Ma, S. Anisotropic damage evolution and modeling for a nickel-based superalloy built by additive manufacturing. *Eng. Fract. Mech.* **2022**, *268*, 108450. [[CrossRef](#)]
65. Pourbabak, S.; Montero-Sistiaga, M.L.; Schryvers, D.; Van Humbeeck, J.; Vanmeensel, K. Microscopic investigation of as built and hot isostatic pressed Hastelloy X processed by Selective Laser Melting. *Mater. Charact.* **2019**, *153*, 366–371. [[CrossRef](#)]
66. Ormastroni, L.M.B.; Lopez-Galilea, I.; Pistor, J.; Rutttert, B.; Körner, C.; Theisen, W.; Villechaise, P.; Pedraza, F.; Cormier, J. Very high cycle fatigue durability of an additively manufactured single-crystal Ni-based superalloy. *Addit. Manuf.* **2022**, *54*, 102759.
67. Rutttert, B.; Ramsperger, M.; Roncery, L.M.; Lopez-Galilea, I.; Körner, C.; Theisen, W. Impact of hot isostatic pressing on microstructures of CMSX-4 Ni-base superalloy fabricated by selective electron beam melting. *Mater. Des.* **2016**, *110*, 720–727. [[CrossRef](#)]
68. Li, Y.; Liang, X.; Yu, Y.; Wang, D.; Lin, F. Review on Additive Manufacturing of Single-crystal Nickel-based Superalloys. *Chin. J. Mech. Eng. Addit. Manuf. Front.* **2022**, *1*, 100019. [[CrossRef](#)]
69. Ramsperger, M.; Singer, R.F.; Körner, C. Microstructure of the nickel-base superalloy CMSX-4 fabricated by selective electron beam melting. *Metall. Mater. Trans. A* **2016**, *47*, 1469–1480. [[CrossRef](#)]
70. Meid, C.; Dennstedt, A.; Ramsperger, M.; Pistor, J.; Rutttert, B.; Lopez-Galilea, I.; Theisen, W.; Körner, C.; Bartsch, M. Effect of heat treatment on the high temperature fatigue life of single crystalline nickel base superalloy additively manufactured by means of selective electron beam melting. *Scr. Mater.* **2019**, *168*, 124–128. [[CrossRef](#)]
71. Tucho, W.M.; Cuvillier, P.; Sjolyst-Kverneland, A.; Hansen, V. Microstructure and hardness studies of Inconel 718 manufactured by selective laser melting before and after solution heat treatment. *Mater. Sci. Eng. A* **2017**, *689*, 220–232. [[CrossRef](#)]